

## A DESIGN METHOD FOR TWO-DIMENSIONAL CASCADES OF TURBOMACHINERY BLADES

M. HART\* AND D. S. WHITEHEAD

*Whittle Laboratory, Department of Engineering, Cambridge University, Cambridge, U.K.*

### SUMMARY

A design method for two-dimensional cascades of turbomachinery blades is presented. A finite element potential flow program is extended to allow fluid to transpire through the blade surface, the displaced surface streamline defining a new blade geometry. The potential changes are related linearly to the transpired flow rates. New surface velocities may then be specified as a function of surface distance, in accordance with boundary layer considerations. Closure and smoothness of the new blade are successfully achieved, while large changes in the blade geometry are possible.

KEY WORDS Turbomachinery Cascades Potential Flow Inverse Design

### INTRODUCTION

The boundary layers on a turbine blade are determined largely by the distribution of pressure on the blade surfaces, for given inlet flow disturbance conditions. Therefore, in order to minimize profile loss, it is desirable that the designer should be able to control the surface pressures while ensuring that the required turning of the flow is achieved. Inverse design methods grant this ability by calculating the blade geometry corresponding to specified surface pressures and inlet flow conditions.

A program for the analysis of flow in cascades using a mesh of triangular finite elements has been described by Whitehead and Grant.<sup>1</sup> This program, called FINEL, is limited to subsonic inlet and outlet flow and to only small supersonic patches on the blade surface. The method has been extended to deal with supersonic flow, and the program, called FINSUP, has been described by Whitehead and Newton.<sup>2</sup> Using a technique of modelling small changes to the blade shape by a transpiration flow through the original blade surface, Cedar and Stow<sup>3</sup> have extended FINSUP to operate in the design mode.

The calculation to be described in this paper uses basically the same transpiration technique as Cedar and Stow,<sup>3</sup> but is an extension of the earlier subsonic program FINEL. It does not therefore include the effects of supersonic flow, or the effects of variation of stream tube height or correction for stream surface curvature. The new features are the ways in which the constraints for blade closure and constant circulation are applied, and the way in which smoothing is applied to correct an intrinsic numerical instability in the method. This enables much larger changes to be made to the blade profile.

---

\* Now of Holset Engineering Co. Ltd, P.O. Box A9, Turnbridge Huddersfield, HD1 6RD U.K.

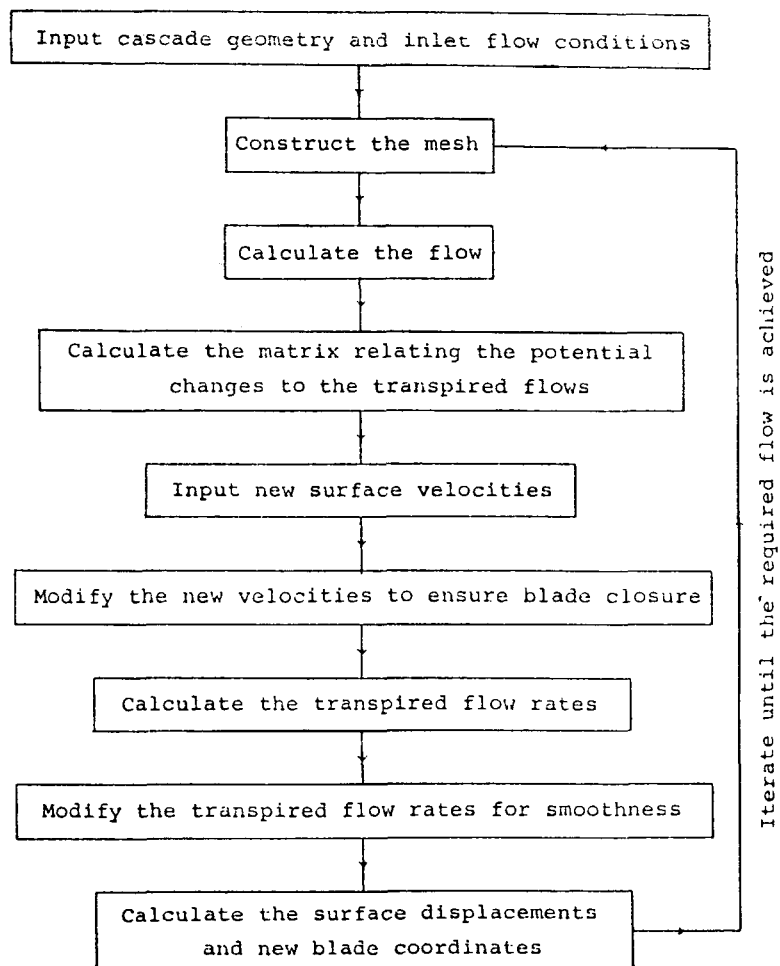


Figure 1. Flow chart of the design procedure

The paper is divided into three main parts. In the first part the flow program is briefly described and the relationship between the changes in the surface potentials and the transpired flow rates is derived. In the second part the design method is described, and in the third part its practical use is explained by way of examples. A flow chart for the whole design procedure is given in Figure 1, to which reference can be made for clarification as each stage is described.

#### THE POTENTIAL FLOW CALCULATION METHOD AND EXTENSION FOR SURFACE FLOW TRANSPARATION

A typical finite element mesh for a turbine cascade is shown in Figure 7. A general point within a triangular element is defined by area co-ordinates  $Z_1$ ,  $Z_2$  and  $Z_3$ , where (see Figure 2)

$$Z_i = A_i/A, \quad i = 1, 2, 3.$$

$A_1$ ,  $A_2$  and  $A_3$  are the areas shown and  $A$  is the total area of the element. The flow is assumed to be two-dimensional and irrotational and therefore may be described by a velocity potential.

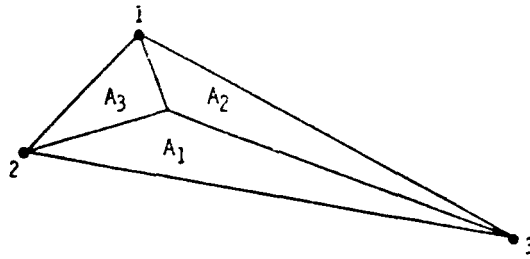


Figure 2. Area co-ordinates

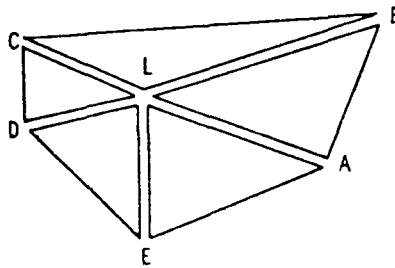


Figure 3. Elements adjoining node L

The potential  $\phi$  is assumed to vary linearly within each element, so that at any interior point

$$\phi = \phi_k Z_k,$$

where  $\phi_k$  gives the values of  $\phi$  at the three nodes of the element. The specific mass flow within an element is given by

$$q_i = \rho V_i = \rho \frac{\partial \phi}{\partial x_i} = \rho \phi_k \frac{\partial Z_k}{\partial x_i}, \quad i = 1, 2, \tag{1}$$

where  $x_1$  and  $x_2$  are length co-ordinates corresponding to the axial and tangential directions. The continuity equation is then

$$\partial q_i / \partial x_i = 0$$

This equation is approximated using the Galerkin technique. Multiplying by  $Z_k$  and integrating over the element for each value of  $k$  gives

$$\int Z_k \frac{\partial q_i}{\partial x_i} dA = 0.$$

Using Gauss's theorem this equation can be transformed to

$$\int n_i q_i Z_k ds - \int q_i \frac{\partial Z_k}{\partial x_i} dA = 0, \tag{2}$$

where the first integral is round the element boundary and  $\mathbf{n}$  is the unit vector normal to the boundary. Now consider all the elements adjoining a node L, as shown in Figure 3. Summing

equation (2) over all these elements, with  $k$  always referring to node L, gives

$$\sum_{\text{elements}} \int n_i q_i Z_k ds - \sum_{\text{elements}} \int q_i \frac{\partial Z_k}{\partial x_i} dA = 0 \tag{3}$$

Now the first term in this equation expresses the flow disappearing down the cracks meeting at L, weighted towards L, and must be set to equal zero for any internal node to represent the continuity equation. The integrand in the second term is uniform over each element, so using equation (1) this becomes

$$\sum_{\text{elements}} \rho \phi_m \frac{\partial Z_m}{\partial x_i} \frac{\partial Z_k}{\partial x_i} A = 0. \tag{4}$$

Since the flow is isentropic, the density  $\rho$  can be expressed in terms of the velocity so that equation (4) becomes a non-linear equation for the unknown values of  $\phi_m$ . This is solved by the Newton-Raphson technique. The correct solution can be expressed as the sum of the current approximation, denoted by  $\bar{\phantom{x}}$ , and a correction term, denoted by  $'$ . Assuming the correction terms are small, terms of second and higher order may be neglected and equation (4) becomes

$$\sum_{\text{elements}} \bar{\rho} A \frac{\partial Z_k}{\partial x_i} \left( \delta_{ij} - \frac{\bar{V}_i \bar{V}_j}{\bar{a}^2} \right) \frac{\partial Z_m}{\partial x_j} \phi'_m + \sum_{\text{elements}} A \frac{\partial Z_k}{\partial x_i} \bar{q}_i = 0,$$

which may be written as

$$\sum_{\text{elements}} K_{km} \phi'_m + \sum_{\text{elements}} F_k = 0. \tag{5}$$

$\bar{a}$  is the local speed of sound. The second term, the flow defect at node L, and the values of  $K_{km}$  are known from the current approximation. The implementation of appropriate boundary conditions is discussed by Whitehead and Grant.<sup>1</sup> Equation (5) may then be used to obtain a converged solution iteratively, starting from a uniform flow equal to the inlet flow.

It has been specified that no flow may pass through the blade surface; that is,  $n_i q_i = 0$ . Using the above framework, it is possible to perturb the converged solution by allowing flow to pass through the blade surface, as shown in Figure 4. Denoting the perturbation by  $'$ , equations (3) and (5) give

$$\sum_{\text{elements}} \int n_i q'_i Z_k ds - \sum_{\text{elements}} K_{km} \phi'_m = 0. \tag{6}$$

The first term in this equation may be written as

$$\sum_{j=1}^{N-1} D_{kj} F'_j,$$

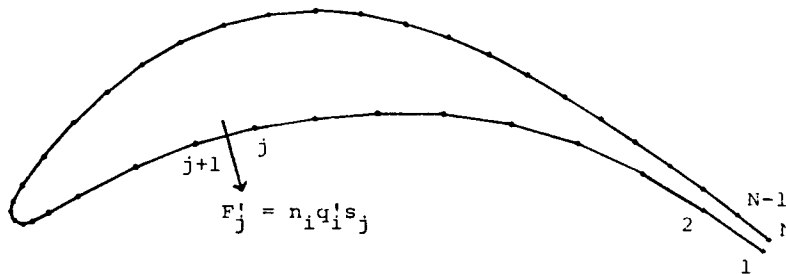


Figure 4. Surface flow transpiration

where  $F'_j = n_j q'_j s_j$ , which, with  $j$  a surface node, is the flow rate through the surface between nodes  $j$  and  $j + 1$ .  $D_{kj}$  is equal to  $\frac{1}{2}$  when  $k = j$  and when  $k = j + 1$  and equal to 0 otherwise.  $s_j$  is the distance between nodes  $j$  and  $j + 1$ .  $N$  is the number of nodes round the blade surface, excluding the node at the end of the cusp.

Equation (6) is then in a similar form to equation (5), only the values of  $\phi'_m$  being unknown. If the values of  $F'_j$  are small, then a good approximation to the modified flow may be obtained from equation (6) and the corresponding equation for each node. A matrix  $\mathbf{J}$  may be determined, linearly relating the potential changes at the nodes to the transpired flow rates:

$$\Phi' = \mathbf{J}\mathbf{F}', \tag{7}$$

where  $\mathbf{F}'$  is an  $(N - 1)$ -dimensional vector.

This relationship opens two possibilities. One could simulate the effect of boundary layers by transpiring fluid through the surface, to achieve a displacement thickness calculated by a boundary layer prediction program. The modifications to the blade surface velocities determined from equation (7) and the boundary layer calculation could be repeated iteratively till convergence was achieved. The displacement effect is important when the boundary layers are thick or separated, which is more likely on compressor blades than on turbine blades.

The second possibility is to use equation (7) to redesign an initial blade, to achieve prescribed potentials at the nodes. The next section is concerned with the detail of the means by which such a design program was developed.

### A DESCRIPTION OF THE DESIGN METHOD

There are  $N - 1$  variables  $F'_i$  corresponding to the boundary sections between the  $N$  surface nodes, excluding the section at the trailing edge. The velocity at the mid-point between nodes  $i$  and  $i + 1$  may be defined by

$$U_i = \frac{\phi_{i+1} - \phi_i}{s_i}, \tag{8}$$

where a positive flow direction is in the direction of  $i$  increasing, as defined in Figure 4. Now define new velocities by

$$U_i^n = U_i + U'_i.$$

Since the velocity field is unchanged by the addition of a constant to the potential field, only new potential differences may be calculated from the new velocities.

Writing

$$\phi_i^n = \phi_i + \phi'_i,$$

equation (8) gives

$$\phi'_{i+1} - \phi'_i = U'_i s_i$$

or

$$\phi'_i - \phi'_1 = \sum_{j=1}^{i-1} U'_j s_j, \quad i = 2, \dots, N. \tag{9}$$

From equation (7),

$$\phi'_i - \phi'_1 = \sum_{j=1}^{N-1} (J_{ij} - J_{1j}) F'_j. \tag{10}$$

Combining equation (9) and equation (10) gives

$$\sum_{j=1}^{i-1} U'_j s_j = \sum_{j=1}^{N-1} (J_{ij} - J_{1j}) F'_j. \quad (11)$$

From this set of  $N - 1$  linear equations, the  $N - 1$  unknown variables  $F'_i$  may be determined by inversion of the matrix  $(J_{ij} - J_{1j})$ , finally giving a relationship of the form

$$F'_i = \sum_{j=1}^{N-1} B_{ij} U'_j, \quad (12)$$

It should be noted that the matrix  $\mathbf{B}$  is independent of the chosen velocity changes,  $U'_i$ , being determined solely from matrix  $\mathbf{J}$  and the surface lengths  $s_i$ .

In order that the mass flow through the cascade should be conserved, and closure of the new blade achieved, it is necessary to satisfy the constraint that the total mass flow through the blade surface should be zero. From equation (12) this requirement becomes

$$\begin{aligned} \sum_{i=1}^{N-1} F'_i &= 0, \\ &\equiv \sum_{i=1}^{N-1} \sum_{j=1}^{N-1} B_{ij} U'_j = 0, \end{aligned}$$

or

$$\sum_{j=1}^{N-1} c_j U'_j = 0, \quad (13)$$

where the constants  $c_j$  are determined by

$$c_j = \sum_{i=1}^{N-1} B_{ij}.$$

Equation (13) effectively removes one degree of freedom from the choice of a new velocity distribution. The following procedure was adopted whereby any chosen velocity distribution could be modified to satisfy equation (13), while maintaining the same circulation about the blade. In order to stay as close as possible to the chosen velocity distribution, an optimization method was used.

It is necessary to determine new velocity changes  $U''_i$  such that

$$\sum_{j=1}^{N-1} c_j U''_j = 0 \quad (14)$$

and

$$\sum_{j=1}^{N-1} s_j U''_j = \sum_{j=1}^{N-1} s_j U'_j. \quad (15)$$

The latter condition ensures that the required circulation and hence the required exit flow conditions are maintained. Consider the function  $f$  defined by

$$f = \sum_{i=1}^{N-1} (U'_i - U''_i)^2.$$

A new set of velocity changes  $U''_i$  may be determined by minimizing  $f$ , subject to the constraints of equations (14) and (15), by using Lagrange multipliers. Define the function  $g$  by

$$g = \sum_{i=1}^{N-1} (U'_i - U''_i)^2 + \alpha \sum_{i=1}^{N-1} c_i U''_i + \beta \left( \sum_{i=1}^{N-1} s_i U'_i - \sum_{i=1}^{N-1} s_i U''_i \right).$$

$g$  can be minimized by setting to zero its derivatives with respect to  $\alpha, \beta$  and  $U'_i$ . Since it may be considered important to keep certain velocities to exactly those values originally specified, this has been made possible. Let there be  $NF$  positions where the velocities are to be fixed to the chosen values, the positions being indicated by the array  $m(i)$ . So,

$$U''_{m(i)} = U'_{m(i)} \text{ for all } m(i), i = 1, \dots, NF.$$

Let the array  $p(i)$  indicate the positions where the velocities may be changed. Then the function  $g$  becomes

$$g = \sum_{i=1}^{NV} (U'_{p(i)} - U''_{p(i)})^2 + \alpha \left( \sum_{i=1}^{NV} c_{p(i)} U''_{p(i)} + \sum_{i=1}^{NF} c_{m(i)} U'_{m(i)} \right) + \beta \left( \sum_{i=1}^{NV} s_{p(i)} U''_{p(i)} - \sum_{i=1}^{NV} s_{p(i)} U'_{p(i)} \right),$$

$$NV = N - 1 - NF.$$

$g$  is now minimized by setting to zero its derivatives with respect to  $\alpha, \beta$  and  $U''_{p(i)}$ , giving  $NV + 2$  linear equations for the  $NV + 2$  unknowns:  $\alpha, \beta$  and  $\{U''_{p(i)}; i = 1, \dots, NV\}$ .

After some algebra, the following result is reached:

$$U''_{p(i)} = U'_{p(i)} - \frac{1}{2}\alpha c_{p(i)} - \frac{1}{2}\beta s_{p(i)}, \tag{16}$$

where

$$\alpha = \frac{2 \left( \sum_{i=1}^{NV} s_{p(i)}^2 \right) \left( \sum_{i=1}^{N-1} c_i U'_i \right)}{\left( \sum_{i=1}^{NV} c_{p(i)}^2 \right) \left( \sum_{i=1}^{NV} s_{p(i)}^2 \right) - \left( \sum_{i=1}^{NV} c_{p(i)} s_{p(i)} \right)^2},$$

$$\beta = \frac{-2 \left( \sum_{i=1}^{NV} c_{p(i)} s_{p(i)} \right) \left( \sum_{i=1}^{N-1} c_i U'_i \right)}{\left( \sum_{i=1}^{NV} c_{p(i)}^2 \right) \left( \sum_{i=1}^{NV} s_{p(i)}^2 \right) - \left( \sum_{i=1}^{NV} c_{p(i)} s_{p(i)} \right)^2}.$$

Clearly there is some arbitrariness to this technique of ensuring mass flow conservation. Its value can only really be assessed by trying it out. In the next section, where experience of using this design method is discussed, an example of the magnitude of the changes given by equation (16) will be presented.

Once the values of the transpiration flow rates  $F'_i$  are all known, it remains to determine the surface displacements, and thus a new blade profile. Firstly, surface velocities  $V_i$  at each node are defined as the derivative with respect to surface distance of a quadratic fitted to the potentials at that node and its two neighbours. The displacements  $d_i$  are then defined as shown in Figure 5 by

$$F'_i = \rho_{i+1} V_{i+1} d_{i+1} - \rho_i V_i d_i. \tag{17}$$

At the leading edge, the stagnation point, as defined by this method of velocity calculation, will lie between two nodes, as shown in Figure 6. It is necessary to decide how to divide the flow  $F'_i$  in order to determine the displacements at these nodes. This was crudely done by weighting the flows with the velocities  $V_i$  and  $V_{i+1}$ , giving

$$\rho_i V_i d_i = \frac{V_i}{V_i + V_{i+1}} F'_i, \quad \rho_{i+1} V_{i+1} d_{i+1} = \frac{V_{i+1}}{V_i + V_{i+1}} F'_i.$$

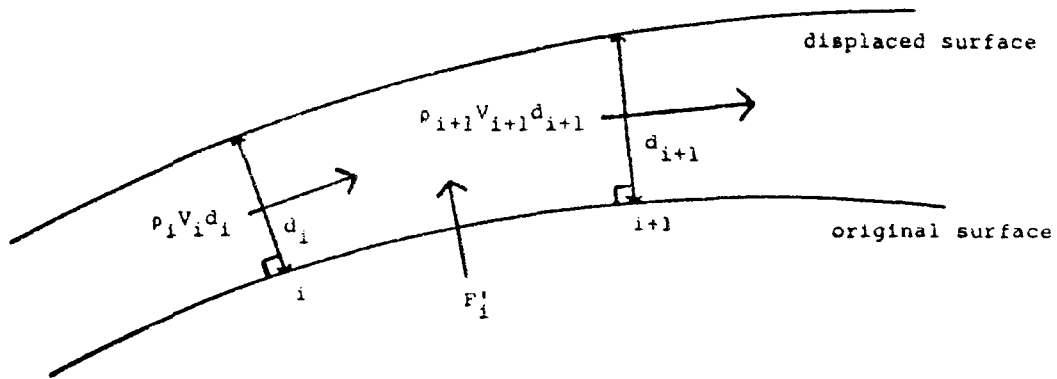


Figure 5. Blade surface displacements

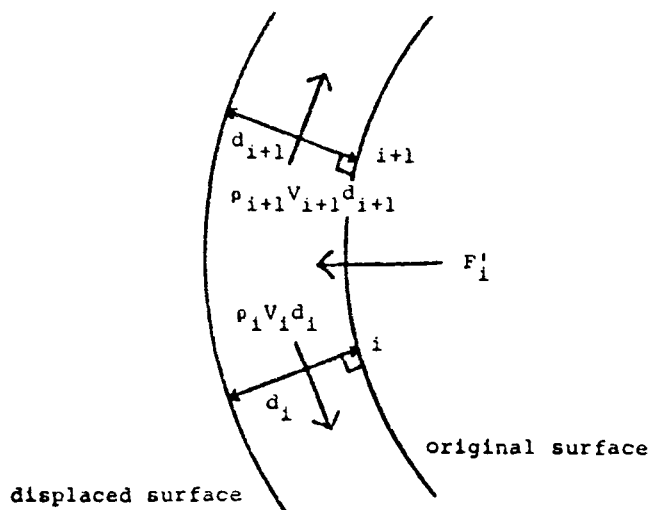


Figure 6. Blade surface displacements at the leading edge

From this start it is then possible to calculate the displacements at each node using equation (17). The displacement at node  $i$  is made along the normal to the quadratic through nodes  $i-1$ ,  $i$  and  $i+1$ . At node 1 the quadratic is fitted through nodes 1, 2 and 3, and at node  $N$  it is fitted through nodes  $N-2$ ,  $N-1$  and  $N$ . A mesh may be generated for the new blade thus obtained, in order to calculate the surface velocity distribution, to compare with the velocities prescribed. In the next section the experience of using this design program is presented.

### EXPERIENCE OF THE DESIGN METHOD

The design method described in the previous section was programmed, and here it will be assessed by considering an example of its use. The initial blade, to be called M1, is shown in Figure 7 in the finite element mesh. The profile was generated by imposing a T6 thickness distribution (see Horlock<sup>4</sup>) on a parabolic camber line. Some details of the geometry and flow conditions are given in Table I.

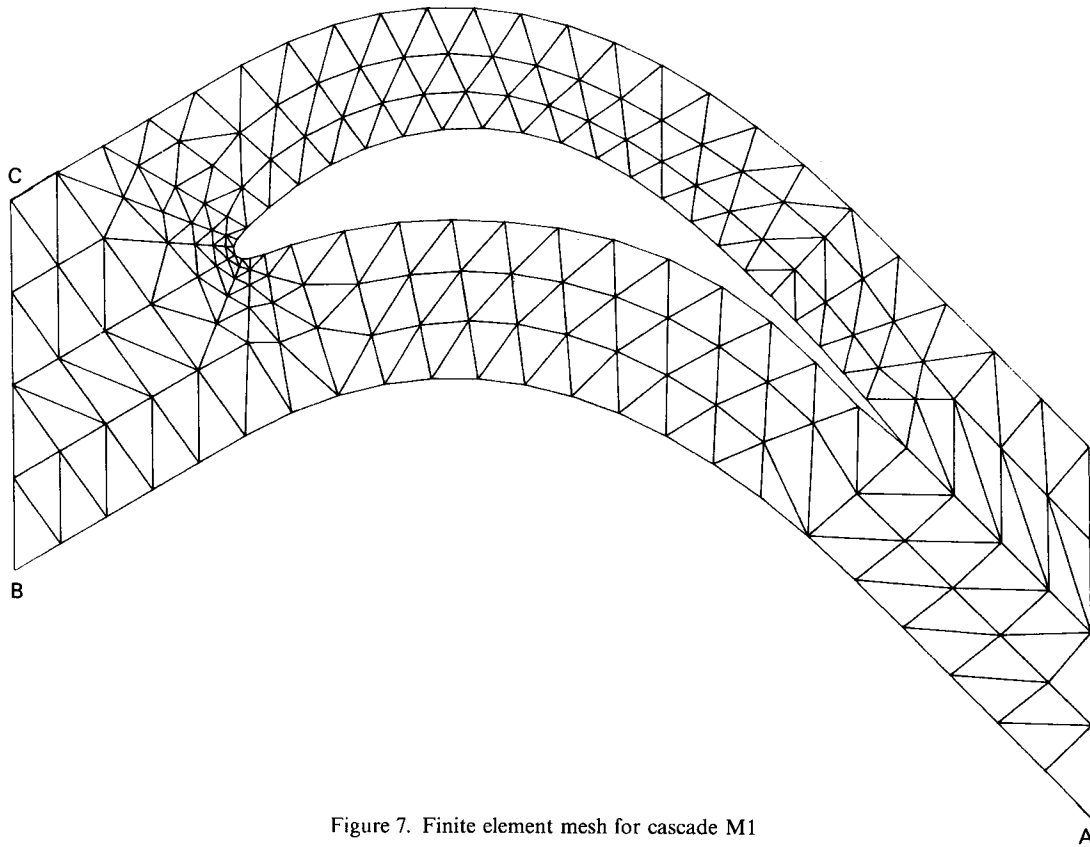


Figure 7. Finite element mesh for cascade M1

Table I

Maximum thickness	15% chord
Pitch/axial chord	0.6
Specified inlet flow angle	30.0°
Specified inlet Mach number	0.4
Calculated exit flow angle	-47.0°
Calculated exit Mach number	0.55
Maximum suction surface Mach number	0.74

Figure 8 shows the calculated surface velocities. In all the plots of velocities to be shown, the symbols represent the mid-points between neighbouring nodes; that is, the positions at which new velocities should be specified. Figure 8 also shows a new velocity distribution chosen to have the same circulation  $C$  as the original distribution, where  $C$  is defined by

$$C = \oint \mathbf{U} \cdot d\mathbf{s} = \phi_{N-1} - \phi_1. \quad (18)$$

By keeping  $C$  constant, the same exit flow conditions should be achieved. The integral in equation (18) is equal to the integral in a clockwise direction around the mesh ABCD in Figure 7. The contributions along AB and CD cancel each other. Far enough upstream and downstream the flow conditions are uniform, so

$$C = h(V_{y1} - V_{y2}),$$

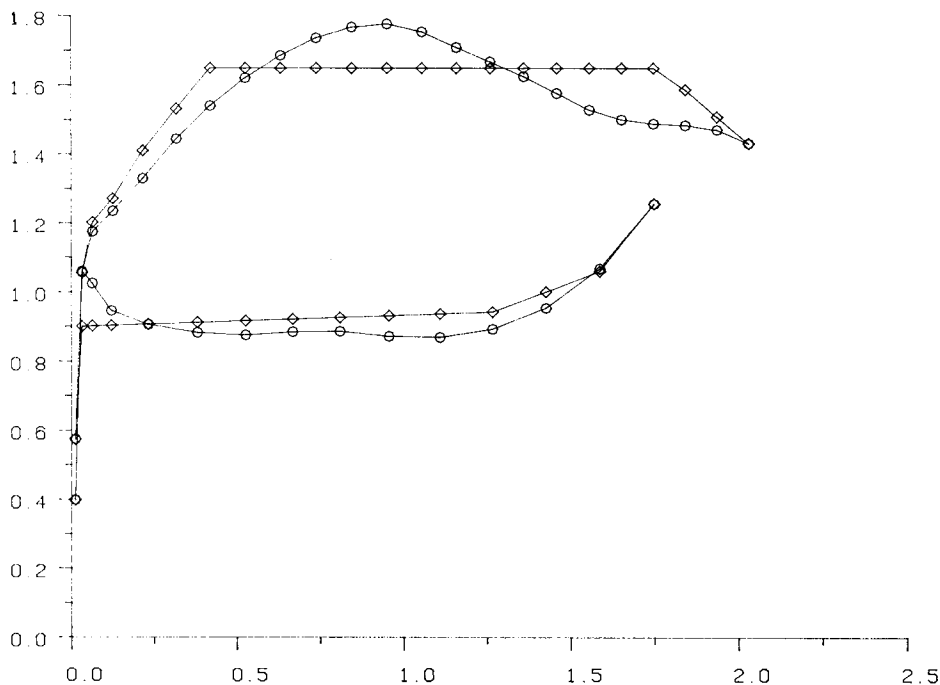


Figure 8. Comparison of calculated and specified surface velocities—original blade. Horizontal axis: surface distance/pitch, Vertical axis:  $U/U_{in}$ .  $\circ$  M1;  $\diamond$  specified new velocities

where  $h$  is the pitch and  $V_y$  is the tangential velocity. Subscripts 1 and 2 refer to the upstream and downstream boundaries respectively. Conservation of mass flow requires that

$$\rho_1 V_{x1} = \rho_2 V_{x2},$$

where  $V_x$  is the axial velocity. Since the flow is isentropic, the density is a function of the local velocity and the inlet conditions. So, given  $C$ , the outlet flow conditions are uniquely determined.

The new velocity distribution in Figure 8 has been chosen merely to demonstrate the use of the design program, not from any loss performance considerations. The next step is to modify these velocities according to equation (16), in order to ensure that the net mass flow through the blade surface is zero. The first and last velocities on each surface were kept fixed and all others allowed to vary. From Figure 9 it can be seen that the modifications are very small.

The new velocity distribution was chosen to maintain the original circulation. However, it is possible to design a new blade having a different circulation. It has been found by experience that, broadly speaking, the greater the change in circulation, the greater are the changes required to ensure mass conservation. When using the program it is therefore advisable to choose an initial blade which gives an outlet flow angle close to that which is required, given the inlet conditions. This is hardly an inconvenience, since it would be somewhat perverse to do otherwise.

A new blade can now be defined by calculating the potential changes, the transpired flow rates, the displacements and then the new co-ordinates. The result is shown in Figure 10. The most striking feature of the new blade is its waviness, particularly on the pressure surface. It may seem reasonable to suppose that this is in some way related to the waviness introduced into the specified velocity distribution in Figure 9, but this is not so. This is an intrinsic instability of the method and can be explained as follows.

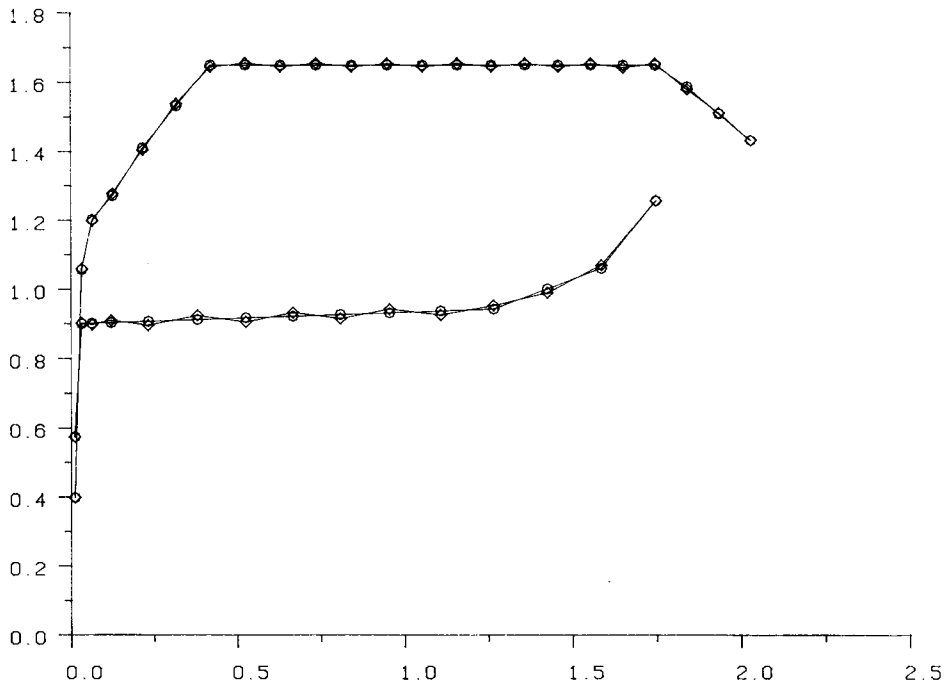


Figure 9. Modification of the specified velocities to ensure blade closure. Horizontal axis: surface distance/pitch. Vertical axis:  $U/U_{in}$ .  $\circ$  New velocities;  $\diamond$  new velocities modified to ensure blade closure

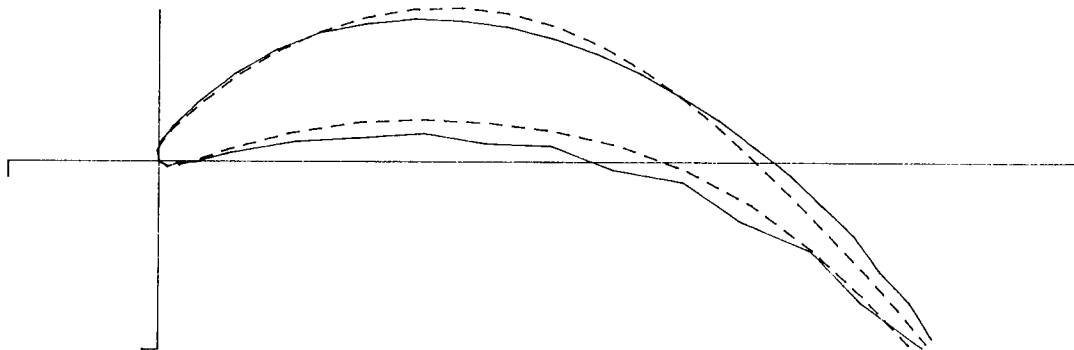


Figure 10. Comparison of the new unsmoothed blade with the original blade: - - - - M1; ——— new blade

Figure 11 demonstrates how a pattern of alternate positive and negative blowing between nodes may have little effect on the potentials at the nodes. This idea was confirmed by finding that the matrix  $(J_{ij} - J_{1j})$  in equation (10) always has a conjugate pair of eigenvalues which are very small compared with all the others. Therefore the matrix  $\mathbf{B}$  in equation (12) has a conjugate pair of large eigenvalues, and for this reason the pattern seen in Figure 11 is easily excited. This is what can be observed in Figure 10.

Clearly it is necessary to eliminate this instability, while recovering the desired displacement. The understanding given by Figure 11 suggests that defining new averaged transpired flow rates  $q_i^n$  in the following manner might help:

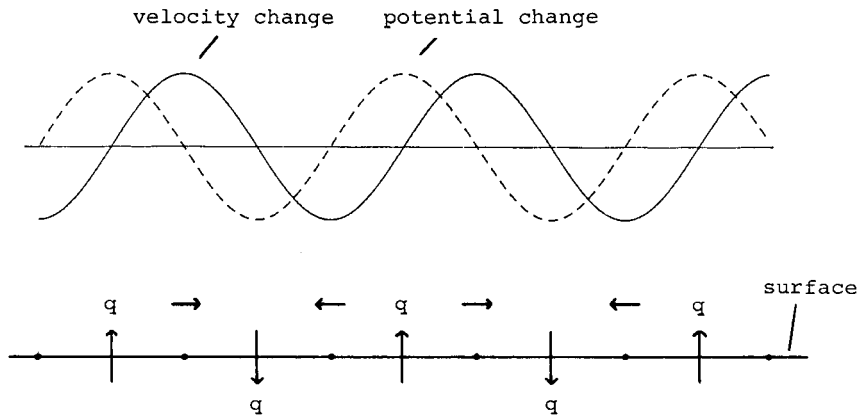


Figure 11. Sketch to illustrate the possibility of large transpired flow rates yet small potential changes

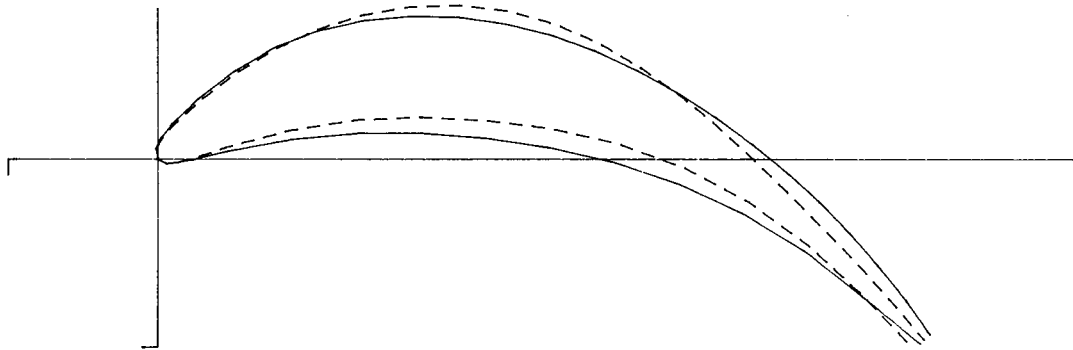


Figure 12. Comparison of the original blade with the first new (smoothed) blade: — M1; - - M2

$$\begin{aligned}
 q_i^n &= \frac{1}{2}[q_i + \frac{1}{2}(q_{i-1} + q_{i+1})], \quad i = 2, \dots, N-2, \\
 q_1^n &= \frac{3}{4}q_1 + \frac{1}{4}q_2, \\
 q_{N-1}^n &= \frac{3}{4}q_{N-1} + \frac{1}{4}q_{N-2}.
 \end{aligned} \tag{19}$$

N.B.

$$\sum_{i=1}^{N-1} q_i^n = \sum_{i=1}^{N-1} q_i = 0.$$

Having done this, a new blade, M2, was obtained and is shown in Figure 12. The desired effect appears to have been achieved, and other cases studied confirm the value of this smoothing technique. Equations (19) are therefore now used routinely and in all further results to be presented.

The flow around M2 was then calculated to compare the surface velocities with those specified. This comparison is shown in Figure 13. The agreement is good after just one iteration. To achieve the required velocities more closely, the procedure was repeated again to give a third blade, M3, compared with M2 in Figure 14. The specified velocity distribution has now been attained with excellent accuracy, as shown in Figure 15. Table II compares the exit flow conditions of the three blades.

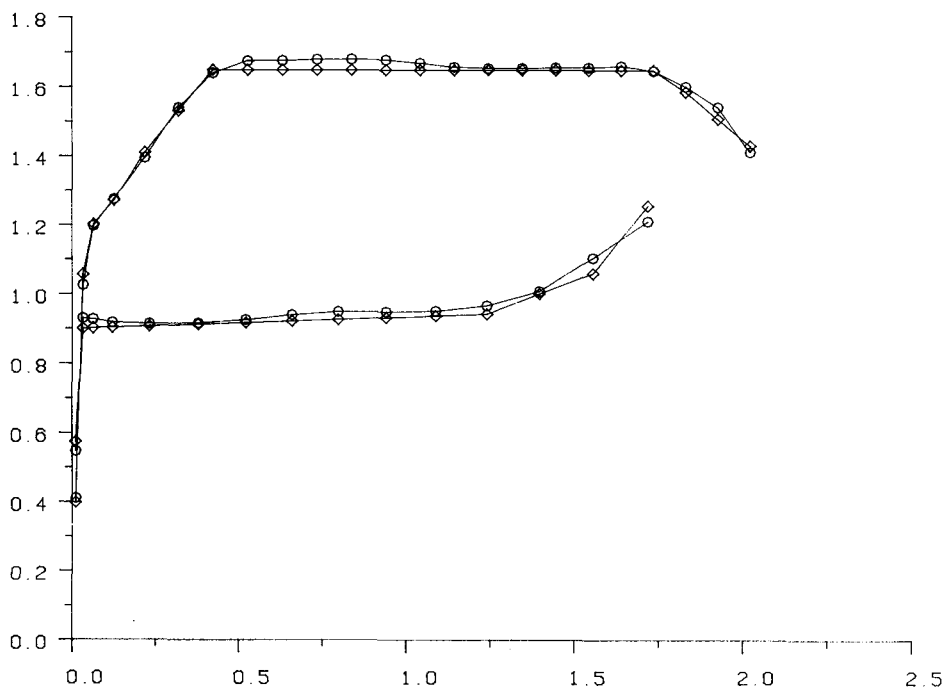


Figure 13. Comparison of calculated and specified velocities—first new blade. Horizontal axis: surface distance/pitch. Vertical axis  $U/U_{in}$ .  $\circ$  M2;  $\diamond$  specified new velocities

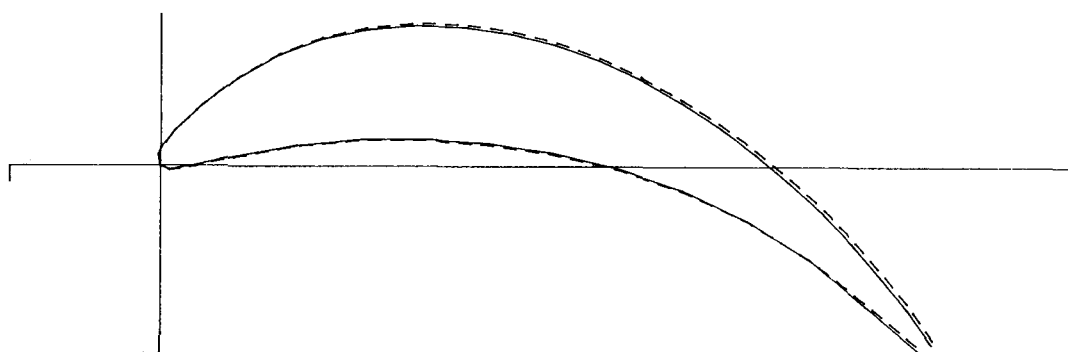


Figure 14. Comparison of the first new blade with the second new blade: ——— M2; ——— M3

The changes in the blade geometry in this example are not large. In particular, the stagger of the blades has hardly changed. The possibility of iteratively approaching the desired solution removes the limit of small changes which a linearized method imposes. It is therefore possible to achieve much larger changes in blade geometry than have been shown above. An example of this will now be given.

The initial profile of the second example, to be called B1, was also generated by imposing a T6 thickness distribution on a parabolic camber line. Some details of the flow conditions are given in Table III. The flow is incompressible.

Figure 17 shows the initial profile and Figure 16 shows the corresponding surface velocity

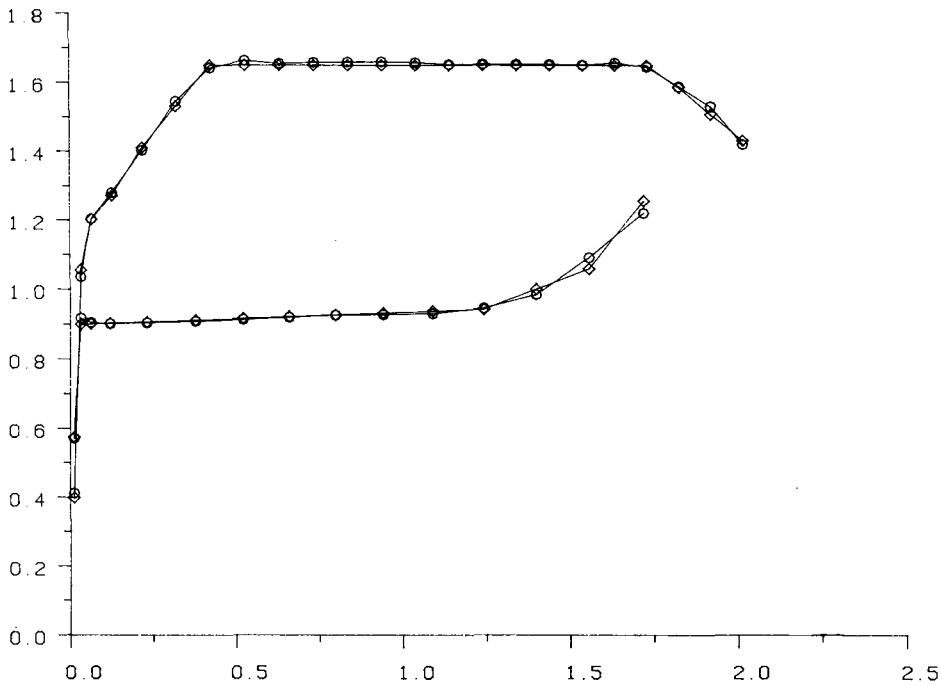


Figure 15. Comparison of calculated and specified surface velocities—second new blade. Horizontal axis: surface distance/pitch. Vertical axis:  $U/U_{in}$ .  $\circ$  M3;  $\diamond$  specified new velocities

Table II

	M1	M2	M3
Exit flow angle	$-47.0^\circ$	$-47.3^\circ$	$-47.3^\circ$
Exit Mach number	0.55	0.56	0.56

Table III

Maximum thickness	10% chord
Pitch/axial chord	0.5
Specified inlet flow angle	$20.0^\circ$
Calculated exit flow angle	$-40.5^\circ$

distribution. New velocities on the pressure surface have been chosen to eliminate any region of deceleration. Beyond the rapid acceleration at the leading edge on the suction surface, the new velocity distribution consists of a region of constant velocity followed by a region of deceleration. The deceleration is such that if the boundary layer is assumed to be laminar, then according to the calculation method of Thwaites<sup>5</sup> the boundary layer will always be on the verge of separation. It has been shown by Hart<sup>6</sup> that if the area under the velocity curve and the velocity at the trailing edge are fixed, then the momentum thickness of the boundary layer at the trailing edge is minimized by such a velocity distribution. The practical limitations of this result are recognized by

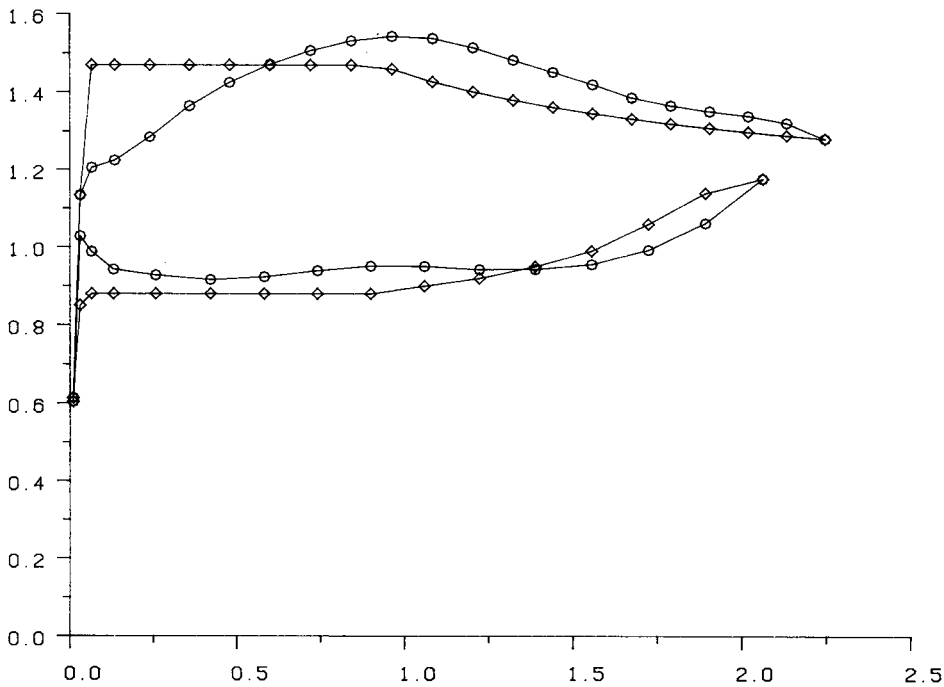


Figure 16. Comparison of calculated and specified surface velocities—original blade. Horizontal axis: surface distance/pitch. Vertical axis:  $U/U_{in}$ .  $\circ$  B1;  $\diamond$  specified new velocities

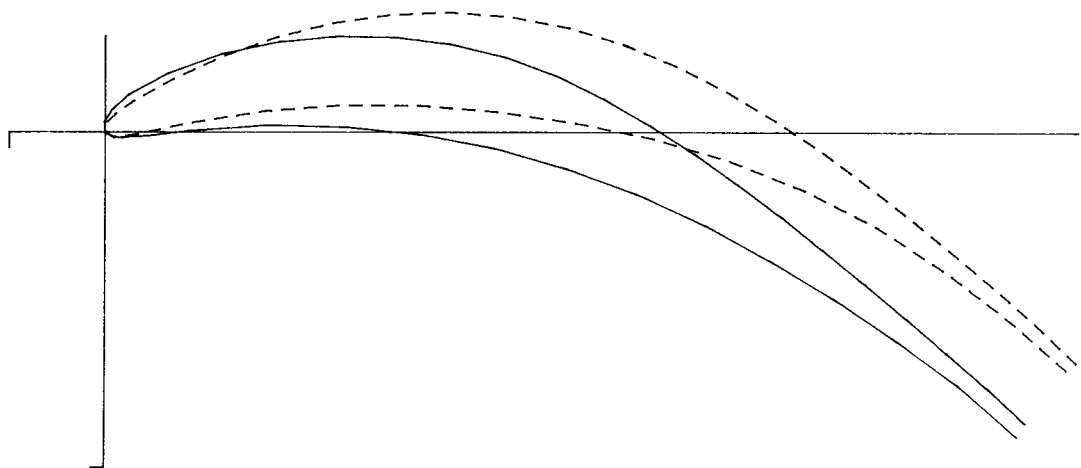


Figure 17. Comparison of the original blade with the first new blade: ——— B1; ——— B2

Hart,<sup>6</sup> and its use here is to illustrate the use of the design method when there is a definite rationale behind the choice of velocity distribution.

The successive modifications to the blades are shown in Figures 17, 19 and 21, from the initial blade, B1, to the final blade, B4. It can be seen from Figure 17 that large surface displacements have been necessary and therefore it is not surprising that an extra iteration was required, compared with the previous example, in order to achieve closely the required velocities. Figures 18, 20 and 22

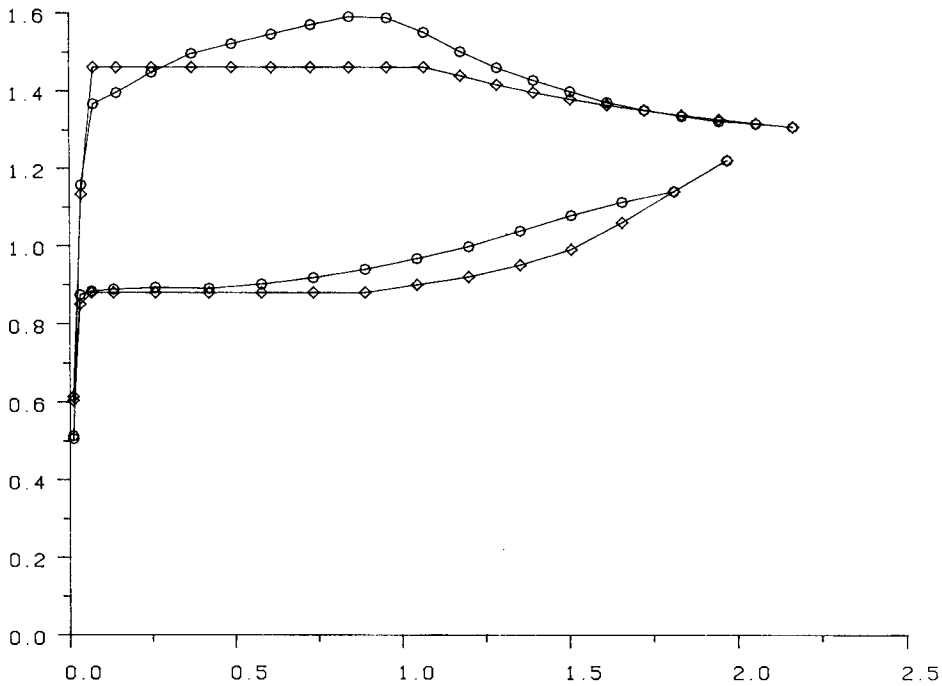


Figure 18. Comparison of calculated and specified surface velocities—first new blade. Horizontal axis: surface distance/pitch. Vertical axis:  $U/U_{in}$ .  $\circ$  B2;  $\diamond$  specified new velocities

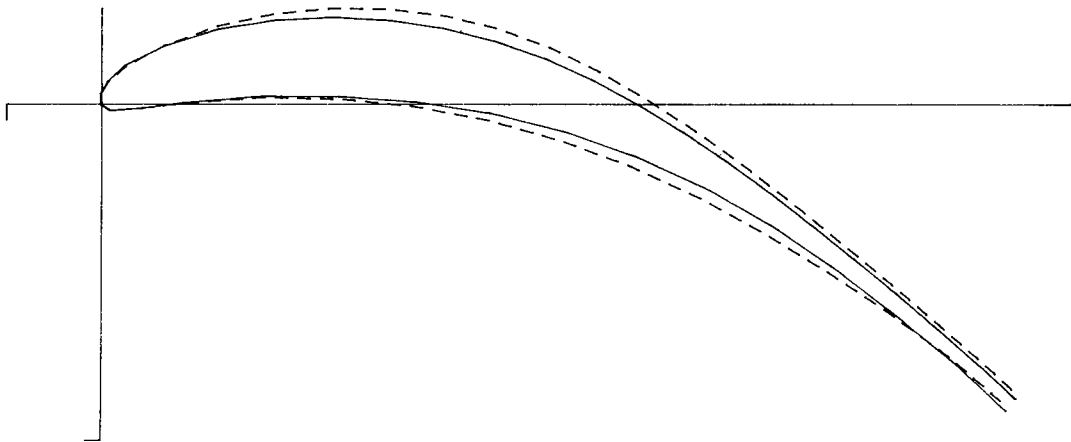


Figure 19. Comparison of the first new blade with the second new blade: ——— B2; ——— B3

compare the specified velocities for blades B3, B4 and B4 respectively with those calculated for the blades B2, B3 and B4.

It may be noticed that there are slight changes in the suction surface velocity distributions specified for the three new blades. Strictly speaking, new velocities are specified between the nodes rather than as a function of surface distance. When a new blade is designed, the surface lengths may change slightly, and the specified velocities would give a different circulation from that required. It

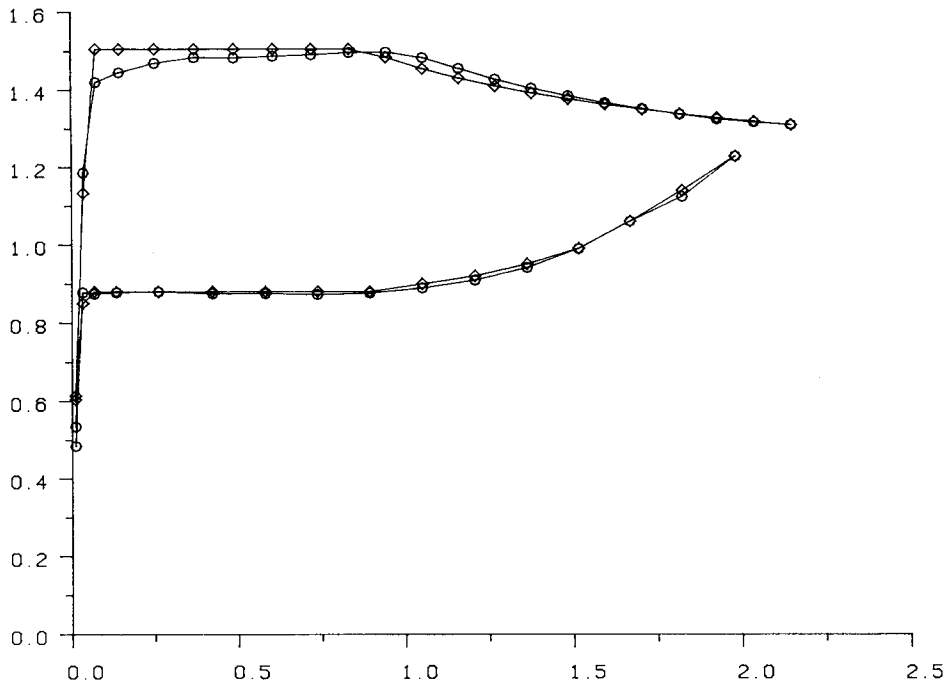


Figure 20. Comparison of calculated and specified surface velocities—second new blade. Horizontal axis: surface distance/pitch. Vertical axis:  $U/U_{in}$ .  $\circ$  B3;  $\diamond$  specified new velocities

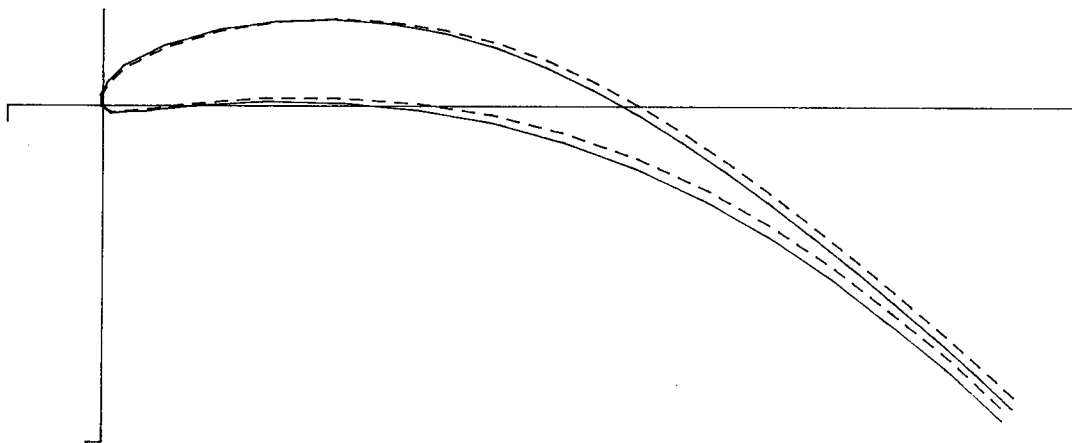


Figure 21. Comparison of the second new blade with the third new blade: - - - B3; — B4

may therefore be necessary to make small changes between iterations to the specified velocities or alternatively to the cascade pitch. This is hardly surprising, since otherwise, for example, one is effectively asking for a fixed ratio of suction surface to pressure surface lengths. The modifications between iterations would depend on the rationale behind the user's choice of velocity distribution and any constraints on geometrical parameters, such as the pitch/axial chord ratio. In this example, the specified velocities on the pressure surface have not been changed between iterations, whereas

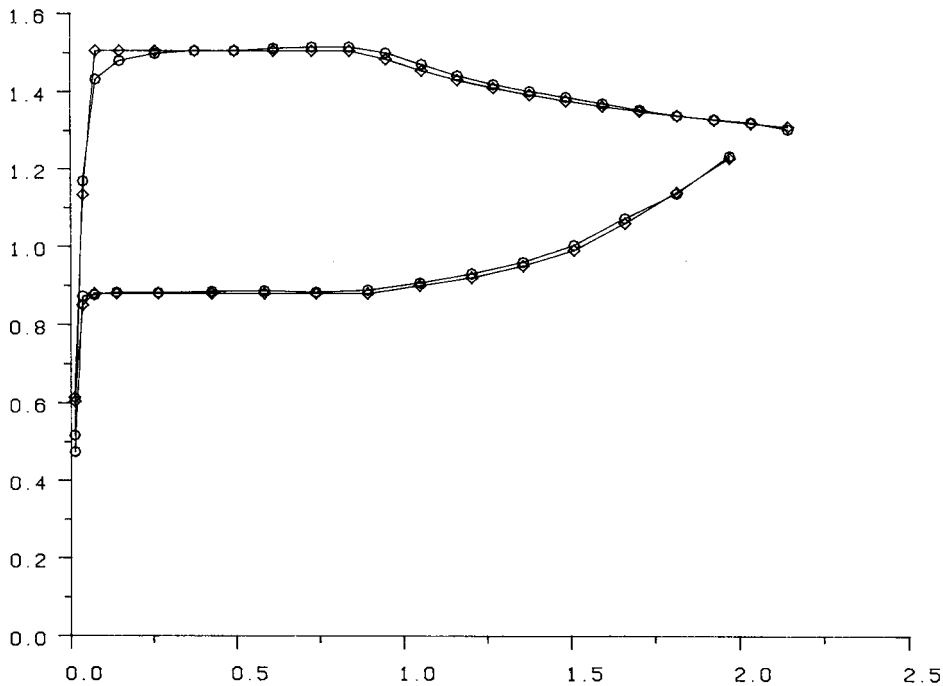


Figure 22. Comparison of calculated and specified new velocities—third new blade. Horizontal axis: surface distance/pitch. Vertical axis:  $U/U_{in}$ .  $\circ$  B4;  $\diamond$  specified new velocities

the specified velocities on the suction surface have been successively modified according to the optimization criterion mentioned above.

The two velocity distributions in Figure 22 agree very well, except near the leading edge on the suction surface, where, as may be expected, the sharp change in velocity gradient could not be achieved. The outlet flow angles for the four blades are: B1,  $-40.5^\circ$ ; B2,  $-40.8^\circ$ ; B3,  $-40.9^\circ$ ; B4,  $-40.9^\circ$ .

It should be noted that the trailing edge thickness is automatically kept nearly constant in this design method, by virtue of the condition that the total mass flow rate through the blade surface should be zero. For, if the transpired flow rate through the suction surface is  $q_s$ , then the total transpired flow rate through the pressure surface is  $-q_s$ . The surface displacements at nodes 1 and  $N-1$  are then given by

$$q_s = \rho_{N-1} U_{N-1} d_{N-1},$$

$$-q_s = \rho_1 U_1 d_1.$$

Since the velocities  $U_1$  and  $U_{N-1}$  will be nearly equal, the displacements  $-d_1$  and  $d_{N-1}$  will also be nearly equal. The displacement directions are roughly similar. It therefore follows that the trailing edge thickness of the blade will remain nearly constant.

## DISCUSSION

The method developed by Cedar and Stow<sup>3</sup> has the advantage that it is not necessary to reconstruct the mesh between iterations, but rather the flow field is resolved, using the Newton-Raphson procedure, with the surface flow transpiration included. However, the closure of the blade

at the trailing edge is achieved by fixing the positions of the trailing edge points and thus effectively fixing the stagger angle. This severely limits the extent to which blade shapes may be modified and the class of specified velocity distributions which are attainable. In the examples given by Cedar and Stow<sup>3</sup> only small modifications to the blade shapes were made compared with the examples shown in this paper.

The processing time required for the design part of the program is typically about half of that required for the flow calculation. The whole program is sufficiently fast to be run interactively on a medium-sized computer. The problems encountered have been overcome satisfactorily, to give a useful engineering tool, if not by a mathematically exact procedure. The important geometric and flow parameters are controllable and the specification of velocities as a function of surface distance facilitates boundary layer considerations. While one is restricted to subsonic flow, the modified version of the flow program, FINSUP, described by Whitehead and Newton<sup>2</sup> is capable of calculating cascade flows which are supersonic at the inlet or outlet. It is envisaged that a similar design method could be developed in this case.

#### ACKNOWLEDGEMENTS

During the period when this work was done, one author, M. Hart, was in receipt of a Co-operative Award in Science and Engineering from the Science and Engineering Research Council in collaboration with Rolls-Royce Limited. Fruitful discussions with R. D. Cedar and P. Stow of Rolls-Royce Limited (Derby) are gratefully acknowledged.

#### REFERENCES

1. D. S. Whitehead and R. J. Grant, 'Force and moment coefficients for high deflection cascades', *Report CUED/A-Turbo/TR98*, Cambridge University Engineering, Department, May 1980.
2. D. S. Whitehead and S. G. Newton, 'A finite element method for the solution of two-dimensional transonic flows in cascades', *Int. j. numer. methods fluids*, **5**, 115-132 (1985).
3. R. D. Cedar and P. Stow, 'A compatible mixed design and analysis finite element method for the design of turbomachinery blades', *Int. j. numer. methods fluids*, **5**, 331-345 (1985).
4. J. H. Horlock, *Axial Flow Turbines*, Butterworth, 1966, p. 74.
5. B. Thwaites, 'Approximate calculation of the laminar boundary layer', *Aeronaut. Q.*, **1**, 245-280 (1949).
6. M. Hart, 'Boundary layers on turbine blades', *Ph.D. Thesis*, Cambridge University, 1985.